CrossMark

Interannual variability of the Arctic freshwater cycle in the second half of the twentieth century in a regionally coupled climate model

Anne Laura Niederdrenk[1] · Dmitry V. Sein[2,3] · Uwe Mikolajewicz[1]

Abstract We use a regionally coupled ocean-sea ice-atmosphere-hydrological discharge model to investigate the influence of changes in the atmospheric large-scale circulation on the interannual variability of the Arctic freshwater (FW) components. This model includes all sinks and sources of FW and allows for the analysis of a closed FW cycle in the Arctic. We show that few atmospheric winter modes explain large parts of the interannual variability of the Arctic FW cycle. A strong Icelandic low causing anomalous strong westerlies over the North Atlantic leads to warmer and wetter conditions over Eurasia. The ocean circulation is then characterized by a strong transpolar drift leading to increased export of FW in liquid and solid form into the North Atlantic. In contrast to this, a weaker than usual Icelandic low and a strong Siberian high is associated with a strong Beaufort Gyre and thus an accumulation of FW within the Arctic Ocean. Not only specific winter conditions but also increased precipitation in late spring and summer, caused by enhanced cyclone activity over land, lead to increased Eurasian runoff, which is responsible for most of the variability in Arctic river runoff.

Keywords Arctic freshwater cycle · Regionally coupled climate model · River runoff variability

✉ Anne Laura Niederdrenk
laura.niederdrenk@mpimet.mpg.de

[1] Max Planck Institute for Meteorology, Bundesstrasse 53, 20146 Hamburg, Germany

[2] Alfred Wegener Institute, Helmholtz Centre for Polar and Marine Research, Am Handelshafen 12, 27570 Bremerhaven, Germany

[3] P.P. Shirshov Institute of Oceanology, Russian Academy of Sciences, 30, 1 Limiya, 199053 St.-Petersburg, Russia

1 Introduction

Observations and model results indicate that the Arctic climate and its FW components change rapidly within the last decades (Meehl et al. 2007). Changes in the FW cycle, such as increased FW export (export of low-salinity ocean water) from the Arctic into the North Atlantic, likely change the thermohaline circulation and consequently might have the potential to influence the global climate (Anisimov et al. 2007). These Arctic FW components show large interannual variability (de Steur et al. 2009; Rabe et al. 2009), that is not well understood so far.

Previous studies conclude that the interannual variability of the FW content within the Arctic Ocean and the FW export from the Arctic into the North Atlantic are strongly regulated by atmospheric dynamics and coupled to changes in the atmospheric large-scale circulation (e.g. Jahn et al. 2010; Proshutinsky et al. 2009; Condron et al. 2009; Zhang et al. 2003; Maslowski et al. 2000). While numerous studies deal with the influence of the variability of dominating pressure patterns on Arctic sea ice (e.g. Tsukernik et al. 2009; Wang et al. 2009; Koenigk et al. 2006; Haak et al. 2003; Rigor et al. 2002), comparatively few studies analyze the impact on liquid FW in the Arctic (Jahn et al. 2010; Karcher et al. 2005; Häkkinen and Proshutinsky 2004). Within these studies the focus is either on the analysis of one specific atmospheric leading mode, such as the Arctic Oscillation (AO) or the North Atlantic Oscillation (NAO) and/or on one specific FW term within the Arctic FW budget, such as the Fram Strait ice export.

We study the impact of different atmospheric leading modes, the first (similar to the AO) and second EOFs of winter mean sea level pressure (MSLP), the NAO and the Siberian high, and thus provide a comprehensive picture of the FW variability in the twentieth century caused by

changes in the atmospheric large-scale circulation. While the defined winter MSLP indexes have a large impact especially on the solid and liquid FW export through Fram Strait and the Canadian Arctic Archipelago (CAA), they do not explain the interannual variability in Arctic river runoff. Using the runoff itself as an index, we investigate the influence from several atmospheric variables on the runoff in the Arctic.

While a coupled climate model can provide continuous time series for several decades and for several FW components, global atmosphere ocean general circulation models show remarkable differences in modeling the Arctic mean climate and the Arctic FW cycle (e.g. Stroeve et al. 2012; Overland et al. 2011; Holland et al. 2010). This is probably caused by the too coarse spatial resolution, which prohibits resolving complex topographic features, such as the CAA, or small scale processes such as slope convection or overflows. Regional ocean models, overcoming the limitation of resolution, agree indeed on the general sinks and sources of the FW budget, but disagree in the magnitude of the mean values as well as on the variability of the FW terms (Jahn et al. 2012). A reason for the differences could be among other things the different resolution of the models or differences in the atmospheric forcing and in the salinity fields. Additionally, these models are uncoupled, thus missing the air-sea interaction. Coupled regional models used for Arctic climate investigations (Döscher and Koenigk 2013; Koenigk et al. 2010; Mikolajewicz et al. 2005) have two disadvantages compared to global coupled models: Firstly, they generally only cover the Arctic Ocean and not the adjacent catchment areas of the rivers draining into the Arctic and thus prescribe the runoff of the Arctic rivers. Secondly, they use salinity restoring or flux correction, and thereby disturb the FW budget artificially. In contrast to these models, our setup includes all sinks and sources of Arctic FW. A global ocean model with highest resolution in the Arctic is coupled to a regional atmosphere model, whose domain covers all catchment areas of the rivers draining into the Arctic Ocean. To provide terrestrial lateral waterflows, we include a hydrological discharge model. Furthermore, we run experiments without any kind of flux correction in the Arctic, which allows, for the first time, for an analysis of a closed FW cycle in high resolution. Due to the comparably large coupled domain, the variability can evolve to a certain extent internally within the model and is not completely externally driven via the forcing at the boundaries of the domain (Sein et al. 2014; Mikolajewicz et al. 2005).

The outline is as follows: In Sect. 2 we describe the model setup and experimental design used for this study. Section 3, the results, is split in three parts, the model validation, with respect to observations and the global model, of the mean state of the FW components in our model (3 3.1), the analysis of the variability of the FW fluxes and the influence of atmospheric leading modes (3 3.2) and the investigation of the drivers of Arctic river runoff (3 3.3). Finally, we give a summary and conclusion in Sect. 4.

2 Model setup and experimental design

Our regionally coupled climate model consists of the global sea ice - ocean model of the Max Planck Institute for Meteorology MPIOM (Marsland et al. 2003) with model grid poles over Russia and North America resulting in high resolution, of approximately 15 km in the coupled domain, in the Arctic Ocean (Fig. 1b). The ocean model has 40 z-coordinate vertical layers with varying thickness between 10 m near the surface and approx. 500 m in deeper layers. A Hibler-type zero-layer dynamic thermodynamic sea ice model with viscous-plastic rheology is included (Hibler 1979). The ocean component is coupled to the regional atmosphere model REMO (Jacob 2001; Majewski 1991), which covers all catchment areas of the rivers draining into the Arctic Ocean (Fig. 1b). The horizontal resolution of the atmosphere model is about 55 km and the model consists of 27 hybrid vertical layers. A similar setup covering the Arctic but in lower resolution was first described in Mikolajewicz et al. (2005) and recently for several domains covering the Arctic, North Pacific and North Atlantic in Sein et al. (2014). To provide lateral terrestrial waterflow, we include the Hydrological Discharge (HD) model (Hagemann and Dümenil 1998). The grid resolution of the HD model is 0.5°. For details on the coupling of the model components we refer to Sein et al. (2015); Elizalde Arellano (2011). External forcing is needed for the ocean model in the uncoupled domain as well as for the atmosphere model at the lateral boundaries. We force our model with output from an experiment performed under historical conditions with the global coupled climate model ECHAM5 / MPIOM in the framework of the Coupled Model Intercomparison Project, phase 3 (CMIP 3). In contrast to reanalysis data, the output of this global model provides a self-contained atmosphere-ocean data-set with its own variability.

As spinup we perform in total 81 years under preindustrial conditions. The initial conditions are taken from a previously performed run. The spinup experiments are run with surface salinity restoring to the sum of the PHC salinity climatology (Steele et al. 2001) and the anomaly of the surface salinity of the global model to its climatological mean. In order to avoid artificial FW fluxes at the river mouth locations (the PHC climatology does not account for FW entering from rivers), we reduce the restoring by inserting an attenuation function in regions with low salinity values, thus especially at coastal areas. For details see Sein et al. (2015) and Niederdrenk (2013). Additionally, the salinity restoring is set to zero in the Arctic to allow

for a closed FW cycle in the Arctic (Fig. 1a). Outside this domain, we use the restoring procedure as explained above. In our production runs, we run the model in the whole coupled domain with FW flux correction instead of salinity restoring, using a climatology of the FW flux correction term calculated from the restoring term from the spinup run. This leads to a completely known, constant, term in the coupled domain, which additionally equals zero in the Arctic and thus provides an undisturbed FW cycle in our region of interest. Outside the coupled domain we use salinity restoring to a surface salinity climatology with a relaxation time of about 77 days. In this analysis we use four experiments, that start in 1960 and end either in 1989 or 1999. They differ in the initial conditions as well as in the climatology of the FW correction. For details of the experiments see Table 1. Even though this is not an ensemble in the classical sense, we count these experiments as members of an ensemble run.

The domain and straits used for our calculation are indicated in Fig. 1a. According to previous studies, the FW budget is calculated relative to a reference salinity of 34.8 (Jahn et al. 2012; Serreze et al. 2006; Aagaard and Carmack 1989). In addition, this is about the mean salinity (= 34.76) in our experiments in the Arctic, in the area

where the ocean is deeper than 1000 m thus excluding the shelves. We calculated the FW budgets also for a mean salinity of 34.7 and conclude that our results are insensitive to the reference salinity, while, of course, the absolute values change.

3 Results

3.1 The Arctic FW cycle

3.1.1 Comparison with observations and the global model

Our model setup shows a realistic mean state of the Arctic climate at the end of the twentieth century. The modeled mean Arctic climate has been validated and compared to observations and reanalysis data in detail in Niederdrenk (2013). The large-scale behavior of atmospheric and oceanic variables is mostly similar to the global model ECHAM 5/ MPIOM, used as boundary conditions. But, particularly in the Arctic sea ice extent and volume, the regional model improved compared to the global model (not shown). In the following, we shortly validate the

Fig. 1 **a** The *light blue domain*, covering the Arctic Ocean, shows the area where the surface salinity restoring is set to zero. Outside this domain we run the model in the coupled domain with a climatological freshwater correction. **b** The computational grids of the model components. The ocean grid is plotted in *blue* and the atmosphere model grid is plotted in *red*. Not every line is shown
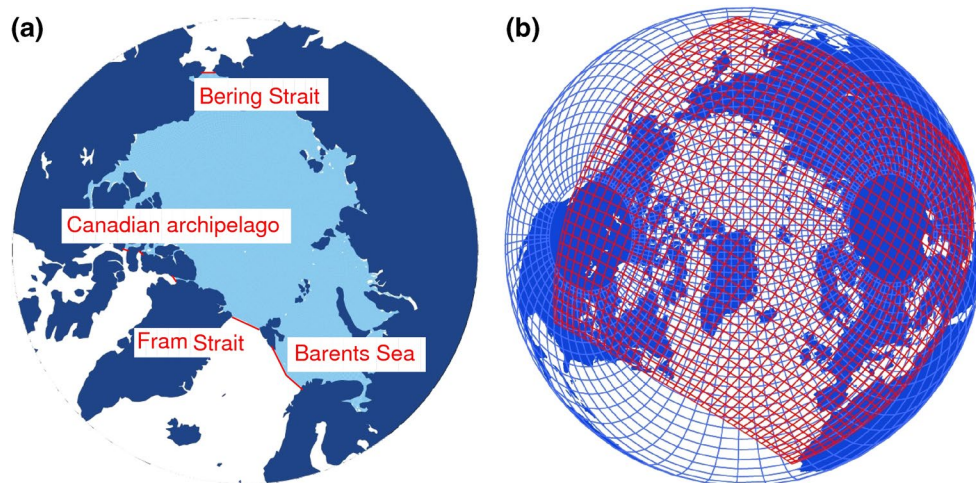

Table 1 List of experiments

	Experiment	Restoring in coupled domain	Restart from	Years
1.	Spinup 1	With salinity restoring set to zero in Arctic	Preexisting exp.	1950–2000
2.	Spinup 2	With salinity restoring set to zero in Arctic	Exp. 1, 12/2000	1970–1999
3.	Production run 1	Without salinity restoring with FW correction term from 2. for 1980–1989	Exp. 2, 12/1999	1960–1999
4.	Production run 2	Without salinity restoring with FW correction term from 2. for 1980–1999	Exp. 2, 12/1999	1960–1999
5.	Production run 3	Without salinity restoring with FW correction term from 2. for 1980–1999	Exp. 4, 12/1991	1960–1991
6.	Production run 4	Without salinity restoring with FW correction term from 2. for 1980–1999	Exp. 5, 12/1991	1960–1991

The experiments 4.–6. were part of a control run with a forcing repetition every 32 years. This is the reason for the run lengths of 1960–1991. The analysis period of these experiments is 1960–1989

Fig. 2 *Left column* Time evolution (yearly values) of the FW components from the regional model and the global model. The ensemble spread is defined by minimum and maximum values of the ensemble members, for liquid and for solid FW transport (in *light red* and *light blue*). Liquid and solid FW transport of the global model is given in *red* and *blue*, respectively. For the last panel, p–e is given in *red* and runoff in *blue*. *Right column* Mean value of the time series of the regional model (ensemble mean) and the global model and from observations and reanalysis data from Serreze et al. (2006)
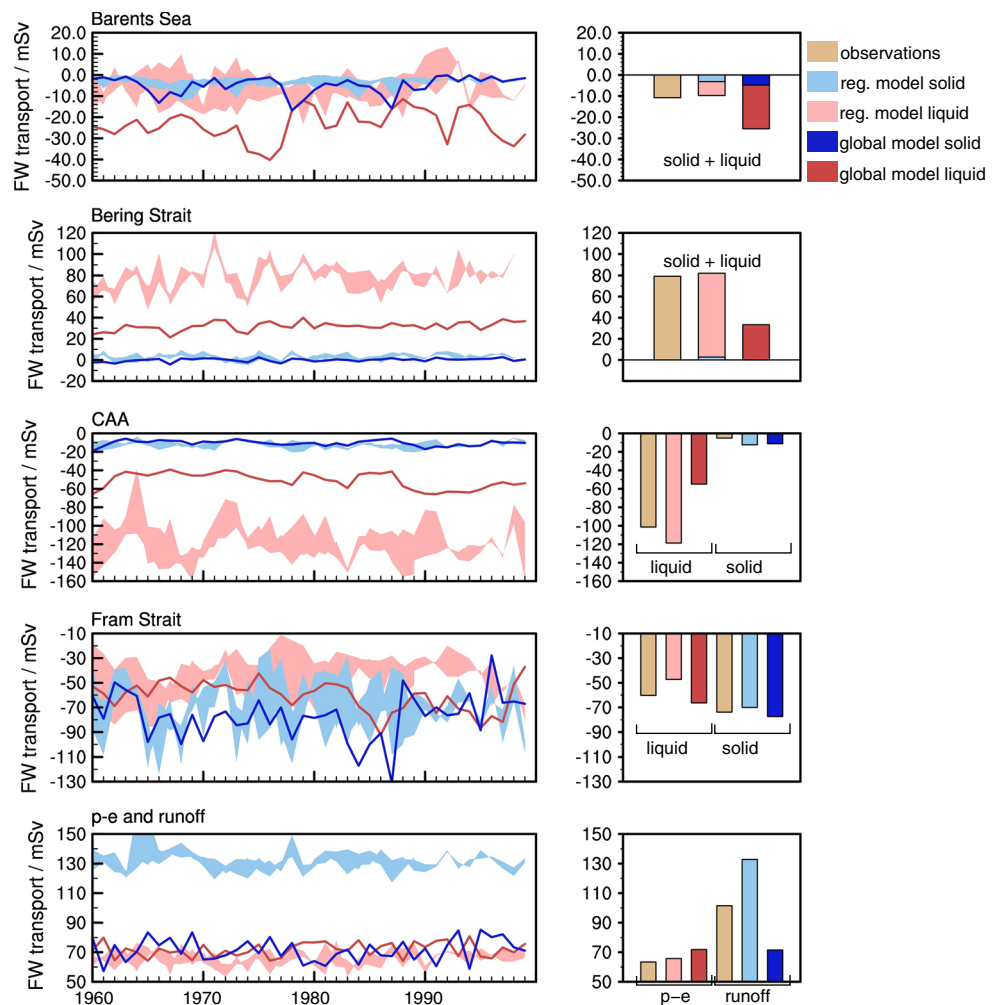
Arctic FW components and their variability with respect to the global model and observations. The time evolution and mean value of the components of the Arctic FW cycle are given in Fig. 2 and the mean values of the regional model and of observational data and reanalysis from Serreze et al. (2006) are presented in Table 2.

The inflow of saline Atlantic water into Barents Sea (Fig. 2a) is estimated to account for −11 mSv of the FW budget (Serreze et al. 2006). The regional model is with −9.7 (±9.3) mSv in the range of the observations, while the Barents Sea inflow in the global model is with −25.5 (±6.7) mSv highly overestimated. However, observations differ largely, Rawlins et al. (2010) combine current-meter mooring data with other measurements and come up with about −27 mSv, which is consistent with calculations from Dickson et al. (2007) stating about −22 mSv as Barents Sea FW export.

The FW inflow through Bering Strait (Fig. 2b) is dominated by the liquid component. In the regional model, the ensemble mean of both, liquid plus solid FW transport, is with about 82.1 mSv very similar to observations, while in the global model, the FW transport into the Arctic through

Bering Strait is underestimated by more than 50 %. The standard deviation of the interannual FW transport through the strait is estimated to be approximately 25–30 % of the total FW transport (Woodgate et al. 2009, 2006). In the regional model, the standard deviation is about 20 % and in the global model, again underestimated, only about 10 % of the modeled total FW transport.

Approximately one third of the total FW is exported through the CAA (Fig. 2c), which is about 100 mSv (Serreze et al. 2006; Prinsenberg and Hamilton 2005). The solid contribution to this amount is only about 5 % (Prinsenberg and Hamilton 2005), because most of the year the ice is landfast. While in our model the FW transport through the CAA (approx. 131 mSv) is overestimated, in the global model the amount of FW transport (approx. 66 mSv) is underestimated . This might be caused by the somewhat lower resolution of the topography of the CAA, but also by a stronger FW export through Fram Strait compared to the regional model.

The transport of FW through Fram Strait is in the regional as well as in the global model consistent with observations (Fig. 2d). The sea ice volume export from our

Table 2 Tabular of the mean values in mSv ($= 1000\,\mathrm{m}^3/\mathrm{s}$) for the fluxes and km^3 for the storage terms of the FW budget of the Arctic from observations and reanalysis data (Serreze et al. 2006) and from modeled data for the years 1960–1999

	Observations	Regional model
(P− E) + runoff	63.4 + 101.5 = 164.9 (±3.5)	65.7 + 132.8 = 198.5 (±12.3)
Bering Strait	79.3 (±9.5)	82.1 (±16.6)
Barents Sea	−11.0 (±2.5)	−9.7 (±9.3)
Fram Strait liquid	−60.0 (±12.7)	−47.2 (±16.8)
Fram Strait ice	−74.0 (±10.8)	−70.0 (±21.8)
CAA liquid	−101.0 (±10.1)	−118.7 (±19.7)
CAA ice	−5.0	−12.4 (±3.6)
Oceanic storage liquid	74, 000 (±7400)	76, 827 (±6951.5)
Oceanic storage ice	10,000	13, 118 (±1128.1)
$\sum$ Transports	−6.8	22.6

Displayed in brackets are error estimates from observations where available and for modeled data one interannual standard deviation. Positive values mean input of FW into the Arctic Ocean (FW sources) while negative values mean export of FW out of the Arctic Ocean (FW sinks). To avoid negative FW volume, the FW storage is calculated ignoring waters saltier than the reference value

ensemble members agrees well with the reconstructed ice volume flux time series (Vinje 2001; Spreen et al. 2009) not only in the amount but also in the year to year variability. However, the modeled variability seems to be somewhat larger than the observations-derived estimates (not shown).

Compared to Serreze et al. (2006), both models overestimate net precipitation over the ocean (Fig. 2e). In the regional model, particularly precipitation over land is overestimated, which directly leads to an overestimation in river runoff (Fig. 2e). Compared to the R-ArcticNET river discharge database (Shiklomanov et al. 2000), especially the Eurasian runoff is overestimated (not shown). However, the modeled interannual variability of Arctic runoff is with about 6 mSv slightly smaller than in observations with about 7.7 mSv. In the global model, runoff is strongly underestimated and is about the same ratio as net precipitation over the ocean (Fig. 2e).

While most general circulation models (coupled atmosphere ocean models as well as ocean only models) agree on the sign of the FW terms, they differ largely in longterm means and variability of the FW components (Jahn et al. 2012). In our model, however, all sinks and sources are well represented and within the range of observations. In comparison with the global model MPIOM / ECHAM 5, especially the FW transport through Bering Strait and CAA are improved, exactly the regions where high resolution is needed to better resolve the complex topography.

3.1.2 Internal model variability

Within the FW transport through Bering Strait, all four ensemble members of the regional model show a similar variability; high correlations between the experiments (ranging between 0.6 and 0.8 depending on the simulations) indicate that the forcing has a large influence on the

variability in the Bering Strait region. The coupled model domain ends south of the Aleutian islands, thus large-scale atmospheric conditions over Bering Strait are mostly prescribed by the external forcing. This is not true for the Fram Strait FW export, where a substantial amount of variability of the liquid and solid export is generated within the model. (The correlations between the four ensemble members range between −0.3 and 0.5 for the liquid, and between −0.1 and 0.4 for the solid FW transport.) The ice export through Fram Strait is mainly determined by local winds (e.g. Tsukernik et al. 2009; Koenigk et al. 2006), generated by the cross-strait air pressure gradient, which is modified internally within the model. The correlations between the FW transport of the experiments through CAA are somewhat larger than through Fram Strait (ranging between 0.3 and 0.5 depending on the simulations), but the variability is also internally driven and depends on changes in the sea surface height difference between the Canada Basin and Baffin Bay.

To find out, what is driving this interannual variability of the FW fluxes, we look at the main patterns of variability of all Arctic FW components.

3.2 Variability of FW fluxes and atmospheric circulation

3.2.1 Modes of FW flux variability

We compute the leading EOFs of the yearly mean FW transports using all ensemble members at the same time (Fig. 3a, b) and the corresponding (normalized) principal component time series (PCs) (Fig. 3c, d). The leading EOF is characterized by a large net FW export (or import), given by large anomalous exports (or imports) through both straits, Fram Strait and CAA. This transpolar

Fig. 3 **a** Leading and **b** second leading empirical orthogonal function (in mSv) of the FW transports, including the net FW flux, in the Arctic. The explained variance is about 33 and 18 %, respectively. The corresponding normalized PCs, obtained by projecting the different ensemble members onto the EOFs, are presented in **c** and **d**
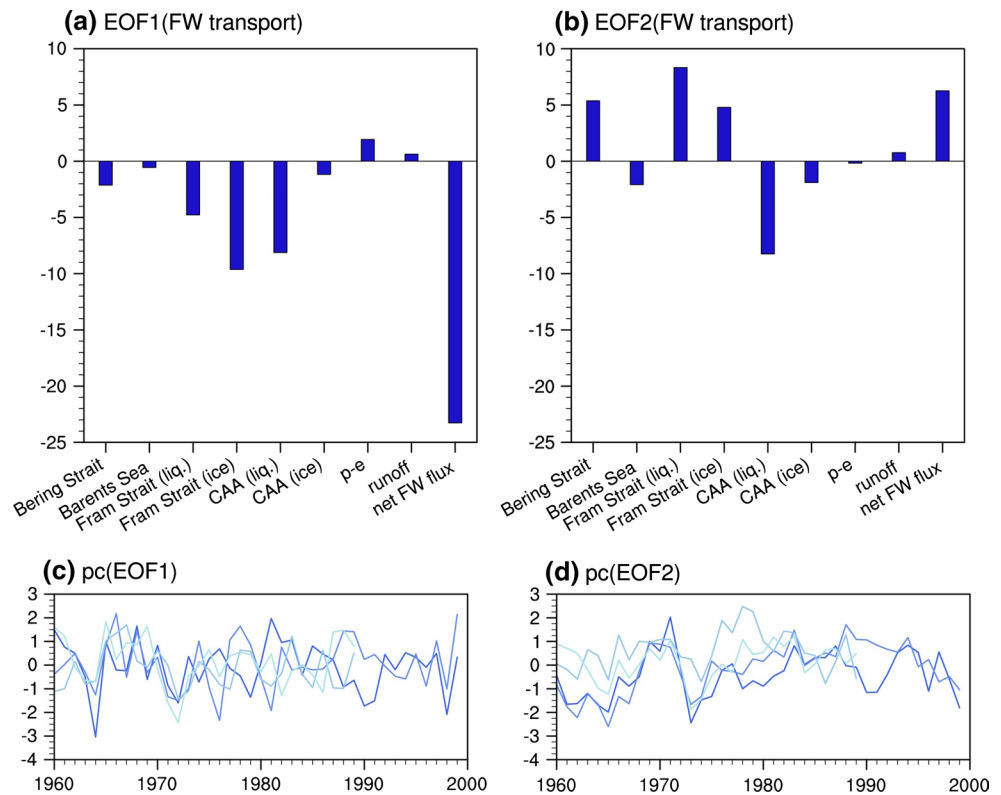
drift anomaly is caused by changes in the atmospheric circulation; the regression coefficient between the PC and near-surface winds shows a shift of the mean winds, from eastern Siberia to northern Greenland and CAA, to winds from the Bering Strait region to Fram Strait (not shown). The second leading EOF of the FW transports is characterized by a reallocation of FW export either through Fram Strait or through CAA, indicating a change in the direction of the FW transport within the Arctic Ocean. While the leading EOF shows a large change in the net FW flux, the second EOF, smaller in its amplitude, shows mainly a change in the pathway of Arctic FW into the North Atlantic, and not in the amount of FW exported to the North Atlantic.

To detect the underlying atmospheric circulation pattern that is responsible for changes of the net FW flux represented in the first EOF, we calculate the regression coefficient between the first PC and MSLP. This regression coefficient (Fig. 4) resembles the leading EOF of winter (= December–February) MSLP (Fig. 5b) and remains highly significant until summer, indicating that this leading pattern of the atmospheric large-scale circulation in winter has a strong impact on the yearly mean FW transports.

In the following, we investigate, which atmospheric circulation patterns are causing changes in the net FW flux in the Arctic. Since drivers can be found in changes of the MSLP in winter, we study, beside the two leading EOFs of

MSLP, also the influence of other winter large-scale circulation patterns on Arctic FW.

3.2.2 Modes of atmospheric variability

The leading EOF of winter MSLP, calculated over a region north of 20°N, is often referred to as the Arctic Oscillation (AO) (Thompson and Wallace 1998; Fyfe et al. 1999). It is characterized by sea level pressure anomalies of one sign in the Arctic and anomalies of the opposite sign in mid-latitudes. Even though our domain of the atmosphere model does not cover the whole northern hemisphere, our leading EOF of MSLP can be interpreted as the AO (Fig. 5b).

A positive trend in AO can be associated with a decrease in MSLP as well as an increase of surface air temperature (Moritz et al. 2002; Morison et al. 2000). However, results from general circulation models do not show a linear behavior in the response of surface air temperature to the AO; the relationship between the AO and variability in the Arctic FW components is not well understood and will be studied in the next subsection.

Additionally, we study the impact of the following climate indexes: The NAO, consisting of two pressure centers in the North Atlantic, also describes the influence of varying pressure gradients over the North Atlantic and its influence on temperature and storm tracks across Europe and
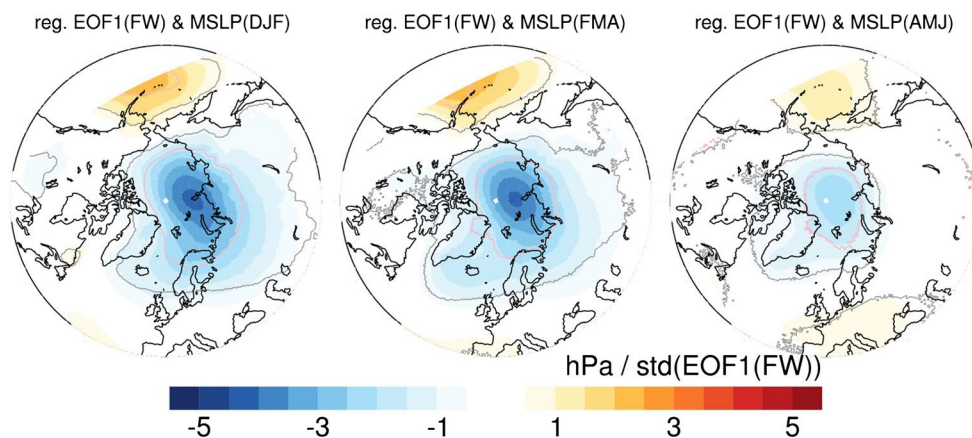
Fig. 4 Regression coefficient between the PC of the first EOF of FW transport and 3 months mean of MSLP in hPa per standard deviation of the PC. DJF refers to the mean value for the period December–February, FMA for February–April and so forth. The *grey contour line* indicates the level of highly significant ($\alpha = 0.01$) values for all model years. The *pink line* indicates the level of highly significant values for 40 years, which is the span of our model simulation 1960–1999 and the minimum of independent model years
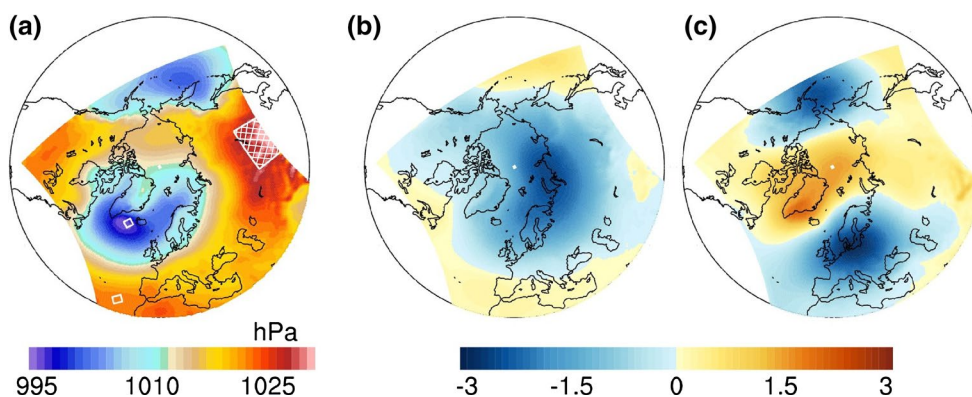

Fig. 5 **a** Winter (DJF) MSLP from the years 1960–1999. Indicated with *white lines* are domains used for NAO index (*without squares*) and for SH index (*squared box*). **b** First and **c** second leading EOF of winter MSLP from the years 1960–1999. EOF 1 explains about 38 % of the total variance, EOF 2 accounts for about 12.8 %

is closely related to the AO. Due to the restriction to the North Atlantic, and the zonally asymmetric pattern, there might be a difference in the physical interpretation and the influence on the Arctic climate compared to that of the AO (Ambaum et al. 2001).

The second leading EOF of winter MSLP in the model is characterized by a tripole pattern (Fig. 5c). We show that this pattern leads to changes in the FW circulation through Fram Strait and into Barents Sea.

Last but not least, we study the influence of the Siberian high (SH), centered in northeastern Siberia. The surface air over land cools while the anticyclonic pressure system forms which leads to some of the lowest temperatures in the northern hemisphere. In our setup, the SH is at the edge of the model domain, so we partly prescribe its strength via the boundary conditions. In our model, the SH has a significant influence on the Arctic FW components, especially

in the years with a stronger and larger than usual high pressure system.

With the above mentioned climate indexes, we perform a composite analysis. By using only years exceeding or underrunning one standard deviation from the mean value (in the following called positive or negative years), we calculate for atmospheric and oceanic components of the Arctic FW budget composite fields and analyze the influence from these extreme MSLP situations on the FW components. This approach has the advantage of monitoring potential nonlinearities between the positive and negative events. The correlation between the indexes of the four ensemble members is high and varies, depending on the defined index and the experiments, between 0.3 and 0.9. Thus, the events for the composites are not fully independent but determined to a certain part by the external forcing.
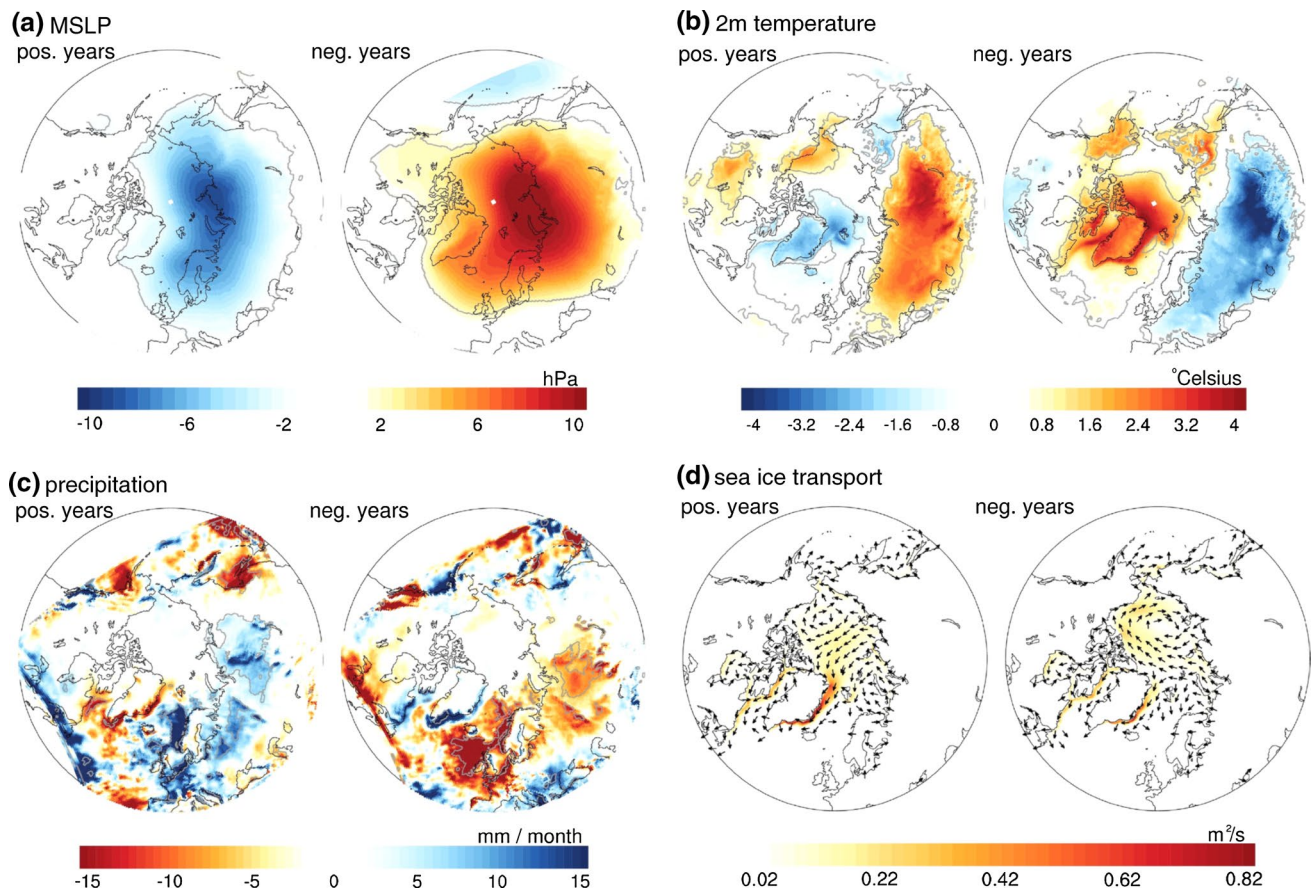
Fig. 6 EOF 1 composites: Difference between DJF mean of the positive years (*left*) and the negative years (*right*) and the overall mean of DJF of **a** MSLP in hPa, **b** 2 m temperature in °C, and **c** precipitation in mm month^{-1}. The *grey contour line* indicates the region where the composite years differ significantly from the mean value. **d** DJF sea ice transport in m^2 s^{-1} in the positive and the negative years. The strength of the velocity vector is given by the color coding

Leading empirical orthogonal function: EOF 1

In the positive EOF 1 years (consisting of 22 years), the Icelandic low is stronger, extending from GIN Sea into Barents Sea, while the weaker than usual Siberian high does not exceed so far northward (Fig. 6a). The stronger than usual low pressure systems arriving from the Atlantic proceed far into Barents Sea and Russia (not shown). For the MSLP in winter, the explained variance exceeds locally 60 % but the influence of EOF 1 on the MSLP pattern decreases after the winter season. The anomalously strong winds from the North Atlantic over Europe into Siberia transport warm and moist air masses from low to high latitudes and the Eurasian continent (not shown), where a surface warming of up to 4 °C (Fig. 6b) and an increase in precipitation over Eurasia (Fig. 6c) can be seen. An overall increased, wind driven, transport (through Fram Strait and the CAA) of FW in solid form leads to a decrease in ice storage in the Arctic.

In contrast to this, in the negative EOF 1 years (consisting of 16 years), a stronger than usual Siberian high pressure system blocks the weaker than usual lows arriving from the Atlantic (Fig. 6a) as well as the eastward transport of heat, allowing for colder than usual temperatures over Eurasia (Fig. 6b). Sea ice is transported in a gyre circulation from the North American coast to the East Siberian Sea (Fig. 6d), leading to a decrease in the total FW transport through Fram Strait by more than 20 % (Table 3), as well as to a decrease through CAA. Thus FW is accumulated within the Arctic Ocean, especially in liquid form.

The signals in net precipitation over land are rather small and so are the differences in the amount of runoff in the EOF 1 composites. The response is largest in the negative years in the outflow of the river Ob, its catchment area is exactly that area where precipitation changes over land are strongest. This reduction in the Eurasian runoff in the negative EOF 1 years leads to a decrease of more than 5 % of the total runoff into the Arctic Ocean.

The FW liquid transport of all years of the upper 100 m and the total FW liquid transport integrated over all depths correlate with 0.9. Hence, nearly all of the FW
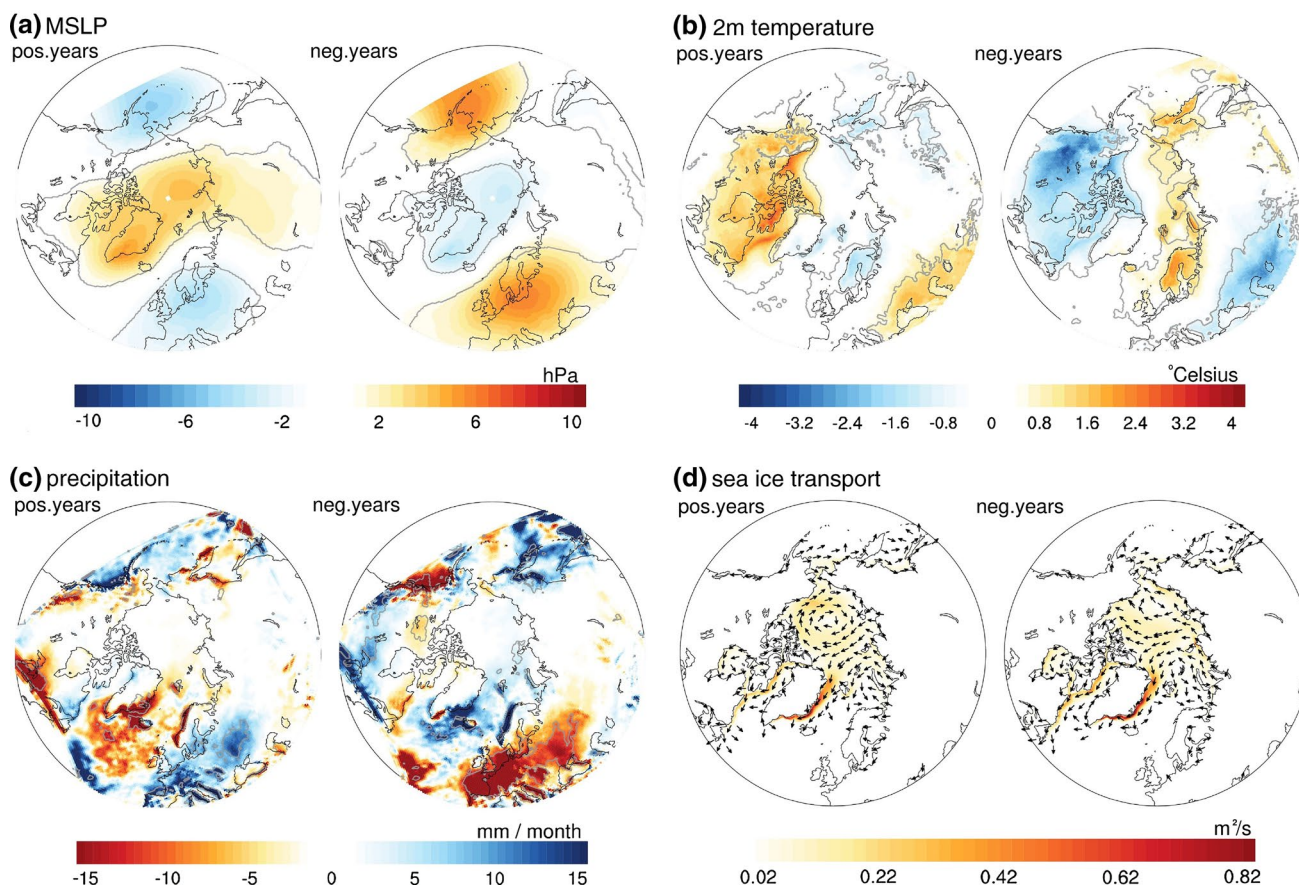
Fig. 7 EOF 2 composites: Same as in Fig. 6, but for the positive and negative EOF 2 years

transport through Fram Strait occurs in the upper layer via the East Greenland current. A decomposition of the FW liquid flux in the upper 100 m through Fram Strait in time mean and time varying parts shows that in the EOF 1 composites the influence of the FW flux due to advection of the mean salinity by the volume flux anomaly has the largest influence on the anomalous mean FW transport. Thus, the increase in the positive EOF 1 years as well as the decrease in the negative years in liquid FW transport through Fram Strait is driven by changes in the total mass transport within the upper 100 m and hence by changes in the wind forcing. Differences in the sea ice transport through Fram Strait are caused by changes in the wind field across the strait (Tsukernik et al. 2009; Koenigk et al. 2006). Following Tsukernik et al. (2009), we calculate a normalized MSLP difference for winter over the strait, that correlates with Fram Strait ice export with 0.7. The absolute MSLP difference for all years equals 7 hPa, for the positive EOF 1 years 12.1 hPa and for the negative EOF 1 years 0.1 hPa. Thus, the stronger than usual gradient in the positive EOF 1 years leads to an increase of ice export through the Fram Strait, while in the negative years the weaker gradient leads to a decrease.

Second empirical orthogonal function: EOF 2

The response of the MSLP pattern in DJF is mostly linear, showing a similar pattern of the anomaly in the positive and negative EOF 2 years with opposite sign. However, in the positive years (consisting of 27 years), the positive signal is extending far into Siberia, while in the negative years (consisting of 24 years), this deviation is more restricted to the Arctic Ocean (Fig. 7a).

In the positive EOF 2 years, a weaker than usual pressure system south of Iceland weakens the heat transport into northern Europe. The stronger than usual Siberian high additionally deflects the warm temperatures southward, leading to a positive anomaly in south-eastern Europe and Central Eurasia. The stronger than usual Aleutian low enhances poleward winds accompanied by high temperatures, leading to a positive anomaly over the North American continent (Fig. 7b). However, the impact on net precipitation in that region is relatively small (Fig. 7c). Changes in precipitation are largest over Europe, where the correlation between the PC of EOF 2 and winter precipitation exceeds 0.8 in large areas. Furthermore, the weaker than usual Icelandic low leads to a decrease in precipitation and an increase in evaporation in GIN Sea and Denmark
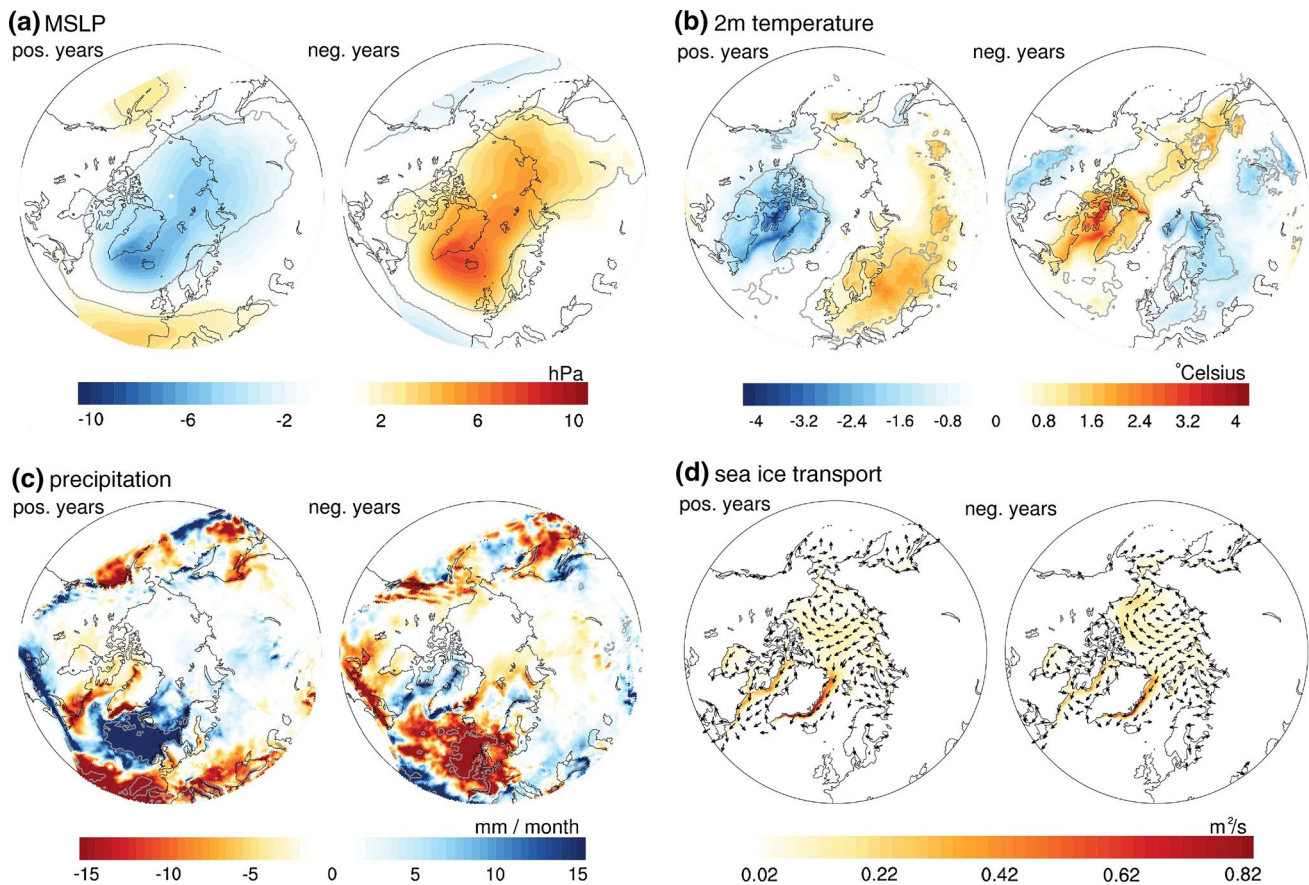
(a) MSLP

pos. years   neg. years

(b) 2m temperature

pos. years   neg. years

(c) precipitation

pos. years   neg. years

(d) sea ice transport

pos. years   neg. years

Fig. 8 NAO composites: Same as in Fig. 6, but for the positive and negative NAO years

Strait. This might be caused by enhanced advection of cold and dry polar air relative to warm moist subtropical air masses. In the Central Arctic and over Russia, changes in net precipitation are small and so is the impact on river runoff. The decrease in (P–E)+runoff (Table 3) is caused by less precipitation over the Arctic Ocean as well as by less runoff from the American continent. However, the signal in the runoff composites is negligible. The FW export, in solid and in liquid form, through Fram Strait and through the CAA, is decreased as well. The liquid FW transport through the archipelago is reduced by about 6 %. Comparable to the negative EOF 1 years, the anticyclonic circulation of the Beaufort Gyre is enhanced, sea ice is transported from the Central Arctic Ocean to the Siberian coast, leading to an accumulation in that area.

In the negative EOF 2 years, the weaker than usual Aleutian low is responsible for lower temperatures over North America, while the stronger than usual Icelandic low leads to a cold anomaly over south-eastern Europe and Central Eurasia (Fig. 7b). Strong transpolar winds lead to an increase in FW export and to a decrease in FW storage, in liquid and in solid form. Sea ice is transported from the Eurasian coast to the CAA and to the North American coast

(Fig. 7d) and is accumulated at the North American coastline, persisting for most of the year. Furthermore, the liquid FW transport through Fram Strait is significantly increased by more than 17 %. In contrast to the positive EOF 1 years, the increase in the total liquid export is not only in the upper 100 m but also in the deeper layers (which equals a decrease of liquid import). This enhanced total liquid export is compensated by an increase of total liquid transport through Barents Sea into the Arctic Ocean. However, the water that enters the Arctic Ocean through Barents Sea is less saline than usual. This leads to a decrease of the Barents Sea saline inflow, even though the total inflow increases. Consequently, the FW transport through the Barents Sea opening, generally a FW sink, is reduced. Additionally, the FW transport is also influenced by an increase in the ice export through Barents Sea into the North Atlantic. Contrary to the EOF 1 composites, the influence on Fram Strait ice export in the EOF 2 composites is comparably small, due to an only small difference of MSLP over the strait.

North Atlantic Oscillation (NAO)

We define the index of the North Atlantic Oscillation as the normalized MSLP difference from the areal means of a region over the Azores high and the Icelandic low (regions
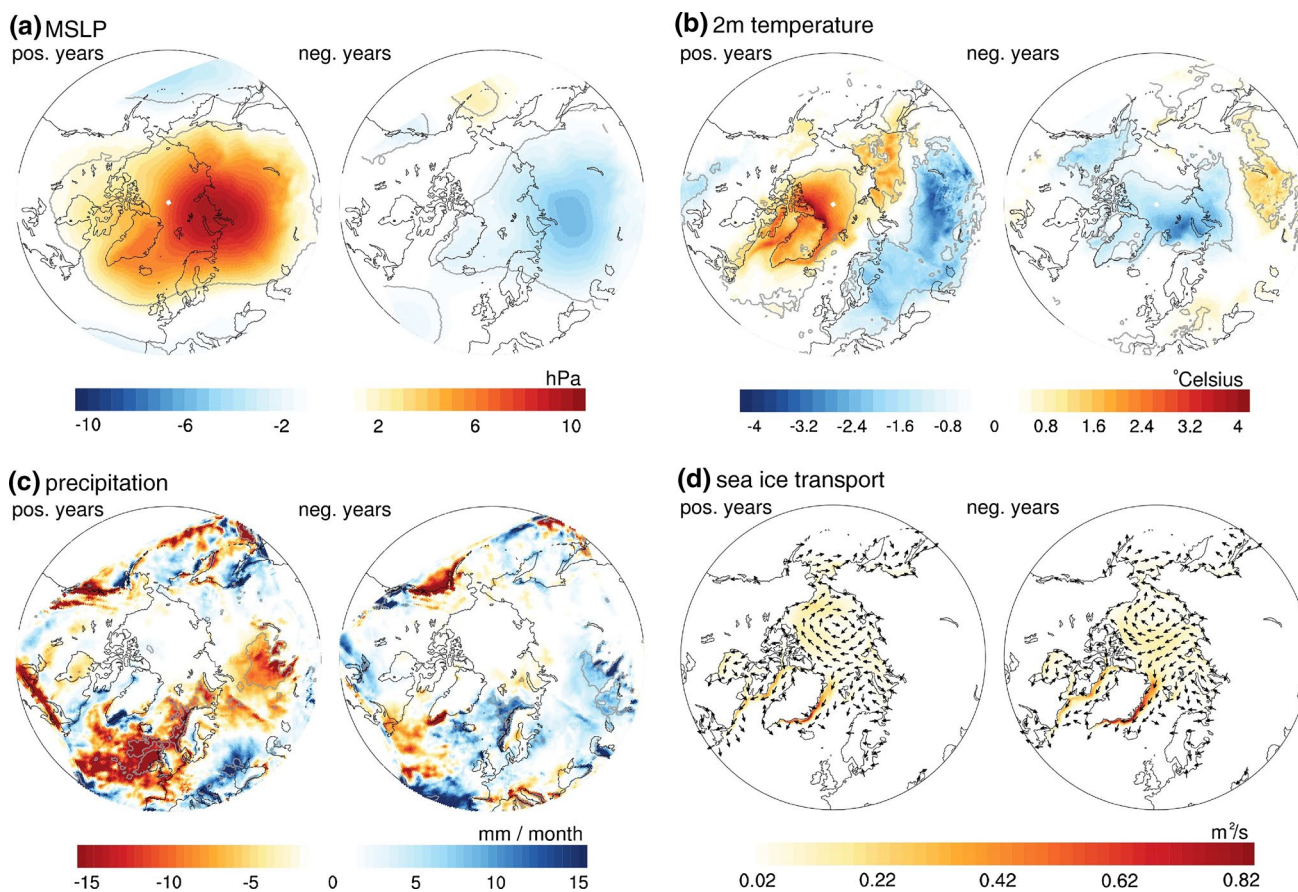
Fig. 9 SH composites: Same as in Fig. 6, but for the positive and negative SH years

indicated in Fig. 5a). Beside a high correlation between the ensemble members, NAO correlates with about 0.5 with EOF 1. In the positive NAO years (consisting of 15 years), a stronger than usual Icelandic low and Azores high, lead to an enhancement of the pressure gradient over the North Atlantic region. In the negative years (consisting of 15 years), the weaker than usual Azores high leads to lower than usual MSLP over Europe. The pattern of the MSLP as well as of the 2 m temperature composites resemble largely the EOF 1 composites, but changes are restricted over ocean and do not extend as far into Eurasia as they do in the EOF 1 composites (Fig. 8a, b). In the positive years, associated with a north-eastward shift of the storm activities over the Atlantic, net precipitation is increased over the Norwegian Sea. In the winter months, the mean value of net precipitation is increased by more than 15 mm month^{-1} in that region (Fig. 8c). Evaporation exceeds precipitation in Labrador Sea and south of Greenland, leading to dryer conditions. The response of net precipitation in the positive NAO years is stronger than in the positive EOF 1. But the positive anomaly over the Norwegian Sea does not extend that far into the northern Eurasian continent. Thus, the influence is weaker over the Arctic adjacent land than it is

in the EOF 1 composites. This is also true for the negative NAO years, where again the influence is largest over the Norwegian Sea and over the eastern North Atlantic. The changes in the model agree well with results from Dickson et al. (2000) having largest precipitation changes in the Norwegian-Greenland Seas and Scandinavia. While changes over Europe are large, the impact on the catchment areas of the rivers draining into the Arctic are small. A difference can be seen only in the Eurasian runoff with an increase of 2.8 % in the positive years. The response is even smaller in the negative years.

As in the positive EOF 1 years, a transpolar drift from Laptev Sea to the Canadian Arctic coast leads to an accumulation of sea ice north of the archipelago and in Lincoln Sea in the positive NAO years (Fig. 8d). In contrast to the negative EOF 1 years, the effect of the enhanced Beaufort Gyre circulation is not present in the negative NAO years. Even though an extension of sea ice in coastal areas in negative NAO years has been observed from ship, aircraft and satellite measurements (Dickson et al. 2000), the response of the model to the negative NAO forcing in the Central Arctic is weak. Although the gyre is enhanced by more than 1 Sv, the sea ice is not pushed strongly enough

Table 3 Mean values in mSv of the FW budget of the Arctic for the positive and negative composite years for EOF 1, EOF 2, NAO and SH

	pos. EOF 1	neg. EOF 1	pos. EOF 2	neg. EOF 2
(P–E)+runoff	65.4 + 132.9 = 198.3 (±2.5)	65.2 + 125.8 = **191.0** (±3.0)	64.7 + 129.4 = **194.1** (±2.1)	66.7 + 132.5 = 199.2 (±2.2)
Bering Strait	83.2 (±3.4)	*87.1* (±4.0)	82.2 (±2.9)	*77.2* (±3.0)
Barents Sea	**−13.6** (±1.6)	*−8.2* (±1.9)	−11.5 (±1.4)	−7.7 (±1.5)
Fram Strait liq.	−49.3 (±3.0)	*−41.4* (±3.6)	**−42.0** (±2.5)	**−54.2** (±2.7)
Fram Strait ice	**−81.1** (±4.0)	**−49.8** (±4.8)	−68.8 (±3.4)	−76.2 (±3.6)
CAA liquid	−120.4 (±3.7)	*−111.0* (±4.4)	**−111.4** (±3.2)	*−125.2* (±3.3)
CAA ice	−12.4 (±0.7)	*−11.2* (±0.8)	−11.2 (±0.6)	−12.6 (±0.6)
Rate of change liq.	−2.8	38.4	17.2	−14.6
Rate of change ice	−12.7	4.3	−3.7	−2.2
∑ Transports	4.7	56.5	31.4	0.5
	pos. NAO	neg. NAO	pos. SH	neg. SH
(P–E)+runoff	67.5 + 134.7 = *202.2* (±3.0)	63.2 + 129.8 = *193.0* (±3.0)	62.2 + 129.0 = **191.2** (±3.0)	64.2 + 133.6 = 197.8 (±2.2)
Bering Strait	85.4 (±4.0)	81.9 (±4.0)	*87.3* (±4.0)	*77.0* (±3.0)
Barents Sea	−10.3 (±1.9)	−11.7 (±1.9)	−8.9 (±1.9)	**−12.8** (±1.5)
Fram Strait liq.	*−42.7* (±3.6)	**−35.6** (±3.6)	−43.6 (±3.6)	−45.7 (±2.7)
Fram Strait ice	*−76.3* (±4.8)	**−59.4** (±4.8)	**−54.0** (±4.8)	*−73.8* (±3.6)
CAA liquid	**−133.2** (±4.4)	−117.2 (±4.4)	**−108.6** (±4.4)	*−122.4* (±3.3)
CAA ice	**−14.8** (±0.8)	−12.0 (±0.8)	*−10.8* (±0.8)	−12.8 (±0.6)
Rate of change liq.	−7.6	12.1	25.9	13.6
Rate of change ice	−3.0	10.4	12.8	0.6
∑ Transports	10.3	39.	52.6	7.3

Values are calculated from the end of September 1 year before the specific event until the end of September of the next year. Displayed in brackets are ± one standard deviation of the subsets. Italic numbers differ more than one standard deviation from the mean value, bold numbers differ more than two standard deviations. The rate of change in storage is calculated as the difference from the end of September until the end of September of the next year. Units are also mSv

to the coastal regions. Changes in the FW stored within the Arctic Ocean are similar to changes in the EOF 1 composites and the signal is consistent with results from Condron et al. (2009); in the positive years, about 10 mSv more FW (liquid + solid) are exported from the Arctic Ocean, while in the negative years, the FW content (liquid + solid) increases by more than 20 mSv.

Siberian high (SH)

We define the Siberian high index by calculating the normalized areal mean of winter MSLP in a region centered in the winter high pressure system over Siberia (region marked in Fig. 5a). Compared with the previously studied indexes, the correlation is highest with EOF 1 and exceeds −0.6.

In the positive years (consisting of 16 years), the Siberian high is extended into the Arctic Mediterranean, covering the complete Arctic Ocean, Greenland and Hudson Bay. Over the ocean, the signal is strongest in Kara Sea and exceeds 10 hPa. Similar to the change in EOF 1 in the North Pacific, but with different sign, the Aleutian low is stronger than usual, while the Icelandic low is weakened (Fig. 9a). The spatial pattern of 2 m temperature is similar to the response in the negative EOF 1 composite,

temperatures decrease by more than 0.5 °C corresponding to one standard deviation of the SH in and around the area, where the high pressure cell is located (Fig. 9b). The strong and largely extended Siberian high leads to less precipitation in the area of index definition. The moisture transport over the Atlantic is weakened and shifted southward (not shown), leading to a negative bias larger than 15 mm month^{-1} over the North Atlantic (Fig. 9c). Thus, the runoff of the river Ob is significantly reduced by about 10 %. This leads to a reduction of the Eurasian runoff, even though the changes in runoff of the other Arctic Eurasian rivers are negligible. The overall influence of SH on the FW fluxes is small, but somewhat larger in the positive years. An enhanced Beaufort Gyre weakens the drift through Fram Strait resulting in a significantly decreased ice export through the strait (Fig. 9d). The FW transport through the CAA is also decreased, more strongly in liquid than in solid form.

In the negative SH years (consisting of 25 years), the influence on MSLP is mainly restricted to Laptev, Kara and Barents Sea. A weaker Aleutian low comes along with a weaker Siberian high, which allows the stronger than usual Icelandic low to expand far into Barents Sea (Fig. 9a). The

Fig. 10 Regression coefficient between Eurasian runoff and 3 months mean of MSLP in hPa per standard deviation of Eurasian runoff. The term SON refers to the mean value for the period September–November from the previous year, NDJ to the mean value for November–January and so forth. *Grey* and *pink contour lines* indicates the level of highly significant values for all model years and for 40 years, respectively
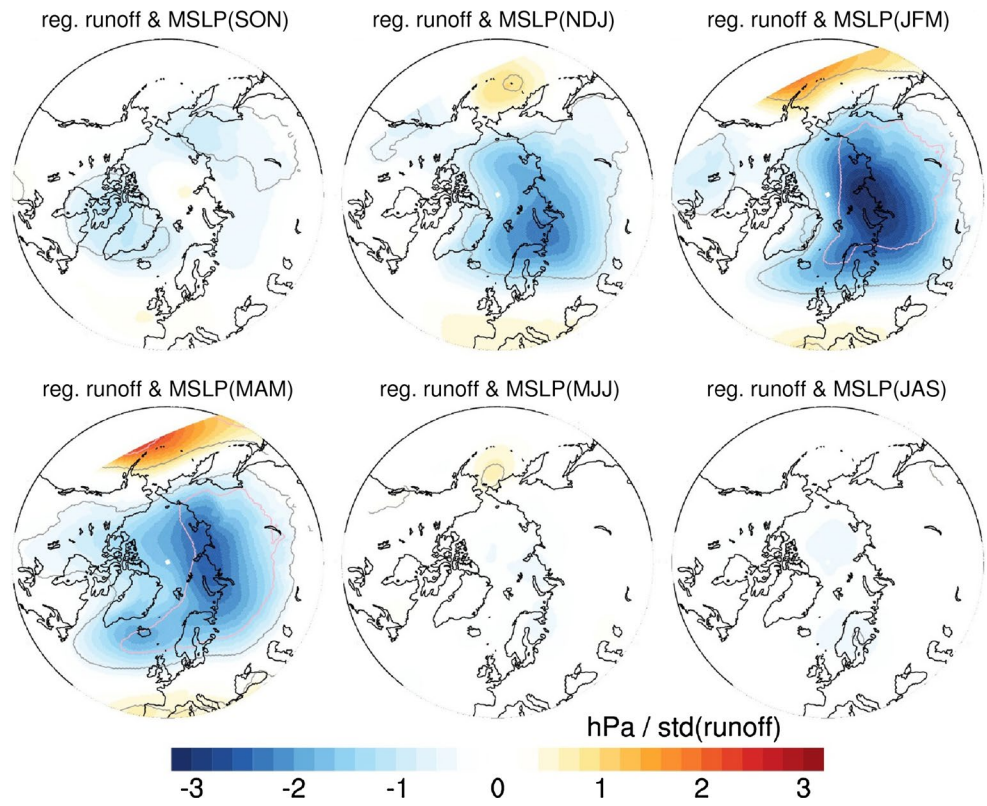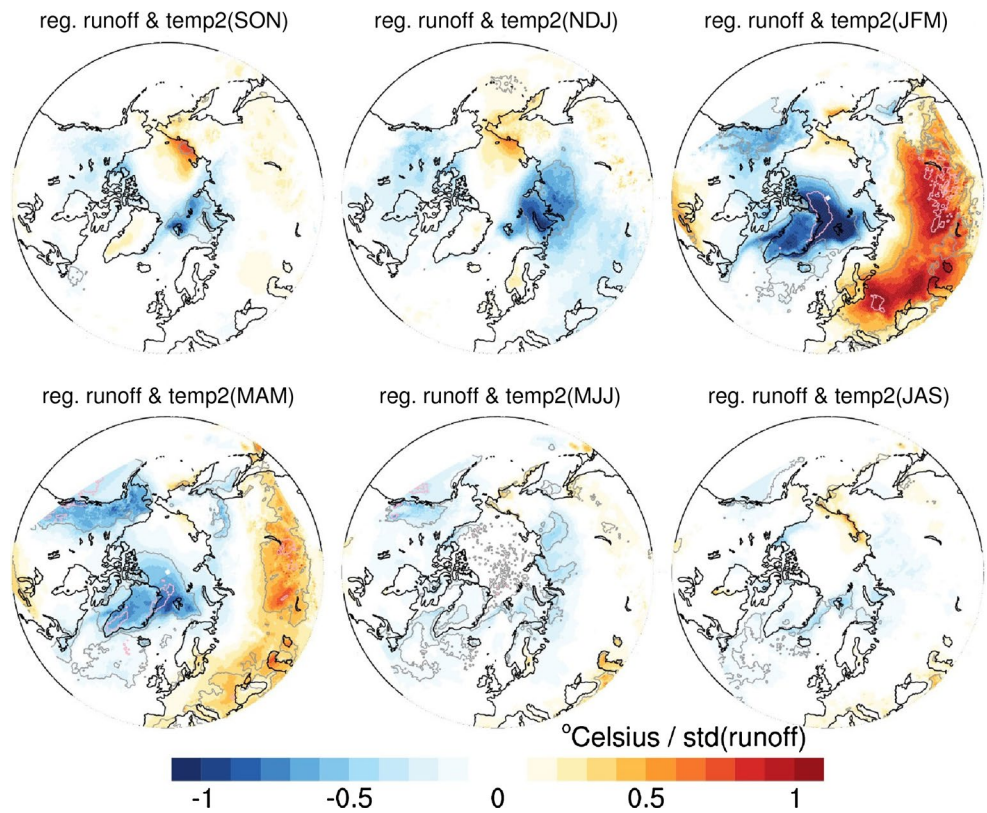
Fig. 11 Same as in Fig. 10, but for 2 m temperature. Units are °C per standard deviation of Eurasian runoff
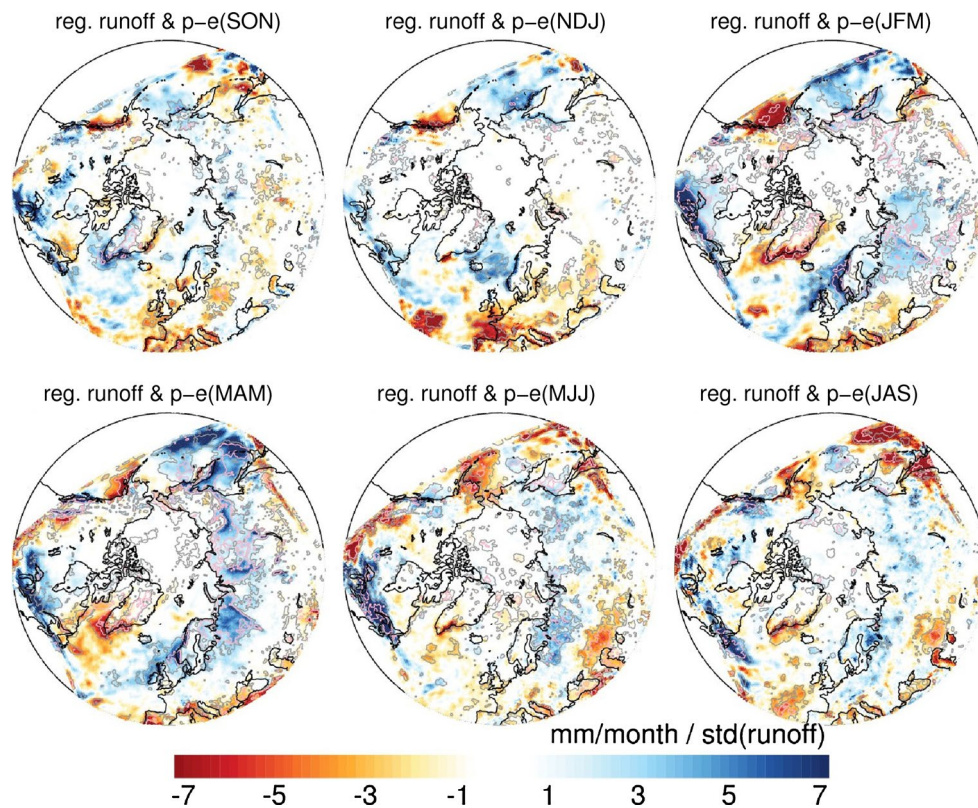
Fig. 12 Same as in Fig. 10, but for net precipitation. Units are mm month^{-1} per standard deviation of Eurasian runoff

2 m temperature, however, does not reflect the pattern of the positive EOF 1 years. The signal over Eurasia is small and primarily restricted to the SH domain. The weaker Aleutian low does not bring as warm temperatures to the North American continent as usual, which leads to a cooling of about 1 °C in Alaska. Even though the Icelandic low is stronger, the enhanced atmospheric heat transport does not reach Barents Sea, but is deflected south. Instead, a cooling can be seen at the winter sea ice edge. Increased sea ice extent leads to a decrease of the heat flux from the ocean to the atmosphere amplifying the cooling over Barents Sea (Fig. 9b). Most probably, precipitation is too much influenced by local winds and other factors to show a large scale significant response on SH. Thus, the influence on runoff is negligible in the negative years. The inflow through Bering Strait is decreased caused by a weaker than usual Aleutian low. On the other hand, the stronger than usual Icelandic low provides an increase in Barents Sea inflow, serving as a FW sink.

To conclude, the changes caused by changes in the strength of the Siberian high are non-linear. While the response of atmospheric and oceanic FW components in the positive years is similar to the response in the negative EOF 1 years, the influence in the negative SH composite is weaker and for all the FW components less than the 95 % criterion of two standard deviations from the mean value.

While the here discussed leading modes of Arctic atmospheric variability account for large parts of the variability of the FW components in the Arctic, none of the indexes can explain the variability in Arctic river runoff. Thus, we focus in the next section specifically on the runoff variability.

3.3 Variability of Arctic river runoff

The variability of the total runoff is dominated by the Eurasian runoff, which is not only larger in the total amount draining into the Arctic Ocean, but also has a larger standard deviation. The correlation between total Arctic runoff and the Eurasian fraction is about 0.9, while the correlation between the total runoff and the North American fraction is negligible.

As we have seen, the atmospheric winter circulation does not preset the conditions for the variability in runoff. To investigate the variability of Arctic runoff, we use yearly mean runoff values and perform a regression analysis with atmospheric datasets from our model. This allows for the analysis of a lagged response to find out which season is important. In the following, we only focus on the Eurasian runoff.

The correlation between MSLP and Eurasian runoff exceeds −0.3 over the Eurasian continent for November to January and
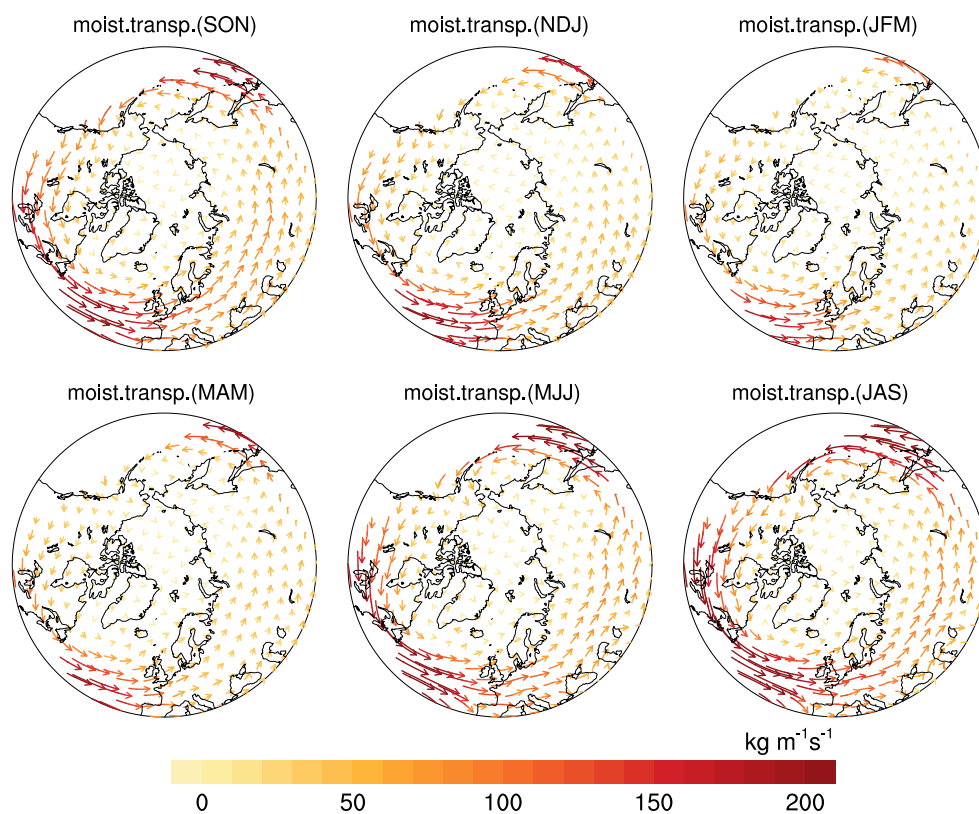
Fig. 13 Vertically integrated mean moisture transport of 6-hourly data in $kg\,m^{-1}\,s^{-1}$. The term SON refers to the mean value for the period September–November, NDJ to the mean value for November–January, and so forth. The strength of the vectors is given by the color coding as well as by its length

reaches about -0.6 in February to April, just before the melting season. In winter, before increased Eurasian river runoff, the Icelandic low is stronger than usual, extending far into Barents Sea and persisting longer than usual (Fig. 10). This causes stronger than usual southwesterly winds to Barents Sea.

An anomalous transport of cold air, transported from Canada over Labrador Sea northward in early winter, leads to a southward shift of the sea ice edge. Thus, less heat release from the ocean to the atmosphere lead to a cooling, first in Laptev Sea and the adjacent coastal area, and in early spring over Greenland and Barents Sea (Fig. 11). The winds bringing warm temperatures over the Atlantic are weaker than usual, while the winds originating over the Canadian continent are stronger and redirected northward (not shown). Even though the circulation regime changes in January to March, bringing warmer temperatures from the south (leading to a warming in large parts of Eurasia of more than 1 °C per standard deviation of Eurasian runoff), the negative temperature anomaly only weakens slowly, vanishing in early summer. In Siberia, the influence of temperature on annual mean Eurasian runoff is small. Hence, the model does not confirm the result of Li et al. (2010) that surface temperature is responsible for most of the explained variance from river Lena.

In winter, the stronger than usual Icelandic low leads to stronger lows arriving from the Atlantic. They are directed more northward than usual, reaching Barents Sea and extending into the Russian continent (Fig. 14) instead of taking the path over Europe (Fig. 13). This leads to increased precipitation during winter of few $mm\,month^{-1}$ in all Eurasian catchments, particularly in the Yenisey catchment. In late winter, the impact on the already small amount of precipitation seems to be restricted to western Eurasia (Fig. 12, upper right panel). From March to May, the weaker than usual Aleutian low allows for more moisture transport along the eastern Pacific coast into eastern Siberia, increasing precipitation also in eastern Siberia (Fig. 12, lower left panel). The influence of precipitation is largest in early summer and explains between 20–30 % of the runoff variability. For all catchment areas in Eurasia, summer precipitation (April to August) increases significantly with up to $6\,mm\,month^{-1}$. Due to warmer than usual temperatures, evaporation also increases, but net precipitation remains increased. In the model, a major driver of the runoff variability is increased cyclone activity in spring and early summer, bringing more moisture than usual in high latitudes (Fig. 14, lower left panel), presumably caused by changes in the polar jet stream track. A
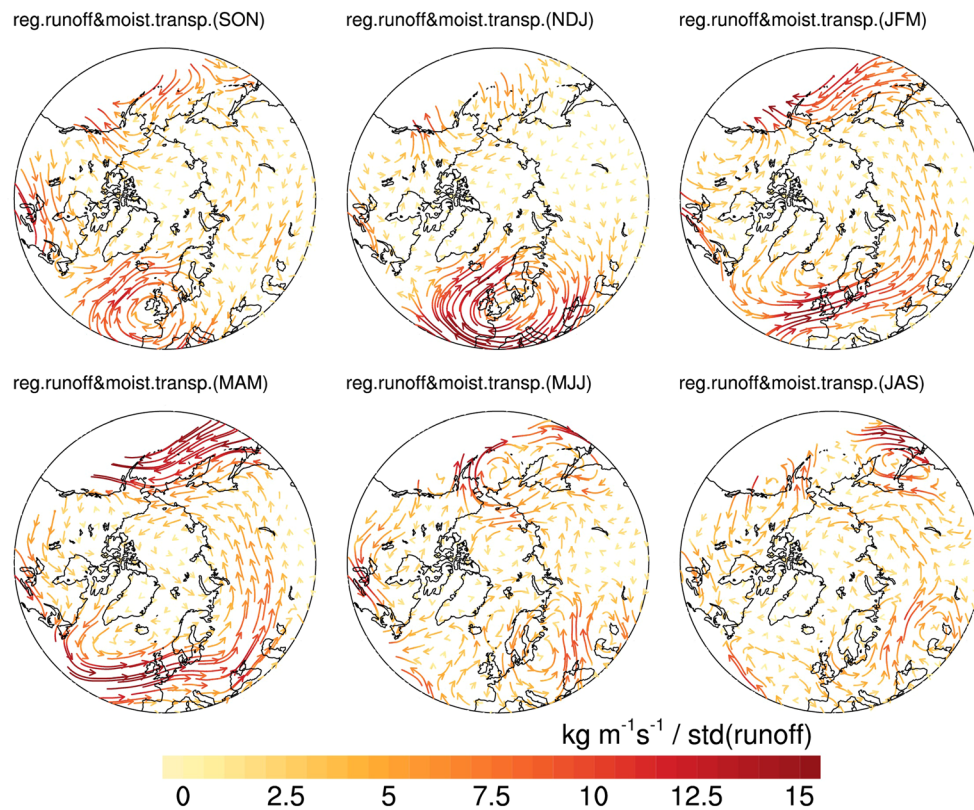
Fig. 14 Regression coefficient between Eurasian runoff and 3 months mean of vertically integrated moisture transport of 6-hourly data in kg m^{-1} s^{-1} per standard deviation of Eurasian runoff

significant strengthening of the polar vortex at 500 hPa as well as at the 200 hPa geopotential height can be seen until early summer in years with enhanced Eurasian runoff (not shown). In January to May (upper right and lower left panel in Fig. 14) especially over land, enhanced activity on a synoptic scale leads to more moisture in Eurasia.

4 Summary and conclusion

With the presented regional model setup, including all sinks and sources of FW in the Arctic, we investigated the influence of specific atmospheric leading modes on the interannual FW variability. Since we run experiments without salinity restoring, the FW budget is not artificially disturbed. While other model studies disagree on the mean value as well as on the variability of the FW components, our results are in good agreement with observations. The Arctic FW components are improved compared to the global model MPIOM / ECHAM 5, especially in the regions where high resolution leads to a better representation of the complex topography.

We have shown that few atmospheric leading modes explain large parts of the interannual variability of the Arctic FW cycle. If the large scale atmospheric circulation in

winter is characterized by a stronger than usual Icelandic low (as in the positive EOF 1 and NAO years as well as in the negative EOF 2 years), anomalous strong westerly winds bring more moisture over the North Atlantic into Eurasia leading to wetter and warmer conditions in northern Europe and Russia. Then, similar to the results from Zhang et al. (2003), the ocean circulation is characterized by a transpolar drift enhancing the FW export, especially in solid form, through Fram Strait and the CAA. On the other hand, a weaker than usual Icelandic low and a stronger than usual Siberian high (as in the negative EOF 1 and NAO years and positive EOF 2 and SH years), are coherent with a strong anticyclonic Beaufort Gyre circulation, leading to a decrease in FW export particularly through Fram Strait and to an accumulation of FW within the Arctic Ocean. At the same time, sea ice is transported and accumulated, depending on the strength and extent of the gyre, either to the Canadian coast or the Siberian coast. Several years of accumulation of FW within the Beaufort Gyre, such as in a recurring negative NAO phase, might be followed by large export events through Fram Strait and the CAA, which then might weaken the strength of the Atlantic meridional overturning circulation. At Fram Strait, liquid FW is mostly transported in the upper 100 m,

an increased export is either caused by increased total mass transport in the upper layer (as in the positive EOF 1 years) or by decreased inflow of salty water in the deeper layers (as in the negative EOF 2 years). Changes in the Nordic Seas, such as large precipitation anomalies as in the NAO years, could thereby also feed back the amount of FW transported through Fram Strait and into Barents Sea (Houssais et al. 2007).

We have shown, that in a winter season before a year with increased Eurasian runoff, an anomalous strong Icelandic low deflects the moisture and heat transport northward taking a shortcut into Siberia. Overall warmer and wetter conditions over the Eurasian continent and increased precipitation during winter, late spring and summer lead to increased river runoff. Especially in early summer, enhanced cyclone activity over northern Europe entering western Siberia is responsible for enhanced precipitation and thus enhanced runoff. Warmer temperatures might lead to the already observed increase in Arctic river runoff, which on the other hand might modify the export of FW through Fram Strait and the CAA and thus the North Atlantic deep-water formation (Peterson et al. 2009). Scenario experiments with this coupled regional setup could provide an inside into the influence of a changing atmosphere on to Arctic FW components and their link to the global ocean circulation.

References

Aagaard K, Carmack EC (1989) The role of sea ice and other fresh water in the Arctic circulation. J Geophys Res. doi:10.1029/JC094iC10p14485

Ambaum MH, Hoskins BJ, Stephenson DB (2001) Arctic oscillation or North Atlantic oscillation? J Clim 14:3495–3507

Anisimov O, Vaughan D, Callaghan T, Furgal C, Marchant H, Prowse T, Vilhjálmsson H, Walsh J (2007) Climate Change 2007: The Physical Science Basis. Contribution of Working Group II to the Fourth Assessment Report of the Intergovernmental Panel on Climate Change, Cambridge University Press, chap Polar regions (Arctic and Antarctic), pp 653–685

Condron A, Winsor P, Hill C, Menemenlis D (2009) Simulated response of the Arctic freshwater budget to extreme NAO wind forcing. J Clim. doi:10.1175/2008JCLI2626.1

Curry B, Lee C, Petrie B (2011) Volume, freshwater, and heat fluxes through Davis Strait, 2004–2005. J Phys Oceanogr 41:429–436

de Steur L, Hansen E, Gerdes R, Karcher M, Fahrbach E, Holfort J (2009) Freswater fluxes in East Greenland Current: a decade of observations. Geophys Res Lett. doi:10.1029/2009GL041278

Dickson R, Osborn T, Hurrell J, Meincke J, Blindheim J, Adlandsvik B, Vinje T, Alekseev G, Maslowski W (2000) The Arctic ocean response to the North Atlantic Oscillation. J Clim 13:2671–2696

Dickson R, Rudels B, Dye S, Karcher M, Meincke J, Yashayaev I (2007) Current estimates of freshwater flux through Arctic and subarctic seas. Prog Oceanogr 73:210–230. doi:10.1016/j.pocean.2006.12.003

Döscher R, Koenigk T (2013) Arctic rapid sea ice loss events in regional coupled climate scenario experiments. Ocean Sci 9:217. doi:10.5194/os-9-217-2013

Elizalde Arellano A (2011) The water cycle in the Mediterranean region and the impacts of climate change. Reports on Earth System Science (PhD thesis)

Fyfe J, Boer G, Flato G (1999) The Arctic and Antarctic oscillations and their projected changes under global warming. Geophys Res Lett 26:1601–1604

Haak H, Jungclaus J, Mikolajewicz U, Latif M (2003) Formation and propagation of great salinity anomalies. Geophys Res Lett. doi:10.1029/2003GL017065

Hagemann S, Dümenil L (1998) Documentation for the Hydrological Discharge Model. Tech Rep 17, Max-Planck-Institut für Meteorologie

Häkkinen S, Proshutinsky A (2004) Freshwater content variability in the Arctic Ocean. J Geophys Res. doi:10.1029/2003JC001940

Hibler W (1979) A dynamic thermodynamic sea ice model. J Phys Oceanogr 9:815–846

Holland MM, Serreze MC, Stroeve JC (2010) The sea ice mass budget of the Arctic and its future change as simulated by coupled climate models. Clim Dyn. doi:10.1007/s00382-008-0493-4

Houssais MN, Herbaut C (2011) Atmospheric forcing on the Canadian Arctic Archipelago freshwater outflow and implications for the Labrador Sea variability. J Geophys Res. doi:10.1029/2010JC006323

Houssais MN, Herbaut C, Schlichtholz P, Rousset C (2007) Arctic salinity anomalies and their link to the North Atlantic during a positive phase of the Arctic Oscillation. Prog Oceanogr. doi:10.1016/j.pocean.2007.02.005

Jacob D (2001) A note to the simulation of the annual and inter-annual variability of the water budget over the Baltic Sea drainage basin. Meteorol Atmos Phys 77:61–73

Jahn A, Tremblay B, Mysak L, Newton R (2010) Effect of the large-scale atmospheric circulation on the variability of the Arctic Ocean freshwater export. Clim Dyn 34:201–222. doi:10.1007/s00382-009-0558-z

Jahn A, y Aksenov, de Cuevas B, de Steur L, Häkkinen S, Hansen E, Herbaut C, M-NHoussais, Karcher M, Kauker F, Lique C, Nguyen A, Pemperton P, Worthen D, Zhang J, (2012) Arctic Ocean freshwater: How robust are model simulations? J Geophys Res. doi:10.1029/2012JC007907

Karcher M, Gerdes R, Kauker F, Köberle C, Yashayaev I (2005) Arctic Ocean change heralds North Atlantic freshening. Geophys Res Lett. doi:10.1029/2005GL023861

Koenigk T, Döscher R, Nikulin G (2010) Arctic future scenario experiments with a coupled regional climate model. Tellus. doi:10.1111/j.1600-0870.2010.00474.x

Koenigk T, Mikolajewicz U, Haak H, Jungclaus J (2006) Variability of Fram Strait sea ice export: causes, impacts and feedbacks in a coupled climate model. Clim Dyn. doi:10.1007/s00382-005-0060-1

Li P, Zhang Y, Liu J (2010) Dominant climate factors influencing the Arctic runoff and association between the Arctic runoff and sea ice. Acta Oceanol Sin 29:10–20

Majewski D (1991) The EUROPA-model of the Deutscher Wetterdienst. In: Conference proceedings; ECMWF Seminar on numerical methods in atmospheric models Vol 2, pp 147–193

Marsland S, Haak H, Jungclaus J, Latif M, Röske F (2003) The Max-Planck-Institute global ocean/sea ice model with orthogonal curvilinear coordinates. Ocean Model 5:91–127

Maslowski W, Newton B, Schlosser P, Semtner A, Martinson D (2000) Modeling recent climate variability in the Arctic. Geophys Res Lett 27(22):3743–3746

Meehl G, Stocker T, Collins W, Friedlingstein P, Gaye A, Gregory J, Kitoh A, Knutti R, Murphy J, Noda A, Raper S, Watterson I, Weaver A, Zhao ZC (2007) Climate Change 2007: The Physical Science Basis. Contribution of Working Group I to the Fourth Assessment Report of the Intergovernmental Panel on Climate Change, Cambridge University Press, chap Global Climate Projections

Mikolajewicz U, Sein D, Jacob D, Königk T, Podzun R, Semmler T (2005) Simulating Arctic sea ice variability with a coupled regional atmosphere-ocean-sea ice model. Meteorol Z 14:793–800

Morison J, Aagaard K, Steele M (2000) Recent environmental changes in the Arctic: A Review. Arctic 53(4):359–371

Moritz RE, Bitz CM, Steig EJ (2002) Dynamics of Recent Climate Change in the Arctic. Polar Sci. doi:10.1126/science.1076522

Niederdrenk AL (2013) The Arctic hydrologic cycle and its variability in a regional coupled climate model. Reports on Earth System Science (PhD thesis)

Overland JE, Wang M, Bond NA, Walsh JE, Kattsov VM, Chapman WL (2011) Considerations in the Selection of Global Climate Models for Regional Climate Projections: the Arctic as a Case Study. J. Clim. doi:10.1175/2010JCLI3462.1

Peterson BJ, Holmes RM, McClelland JW, Vörösmarty CJ, Lammers RB, Shiklomanov AI, Shiklomanov IA, Rahmstorf S (2009) Increasing River Discharge to the Arctic Ocean. Sci. doi:10.1126/science.1077445

Prinsenberg S, Hamilton J (2005) Monitoring the volume, freshwater and heat fluxes passing through Lancaster sound in the Canadian Arctic Archipelago. Atmos Ocean 43:1–22

Proshutinsky A, Krishfield R, Timmermans ML, Toole J, Carmack E, McLaughlin F, Williams WJ, Zimmermann S, Itoh M, Shimada K (2009) Beaufort Gyre freshwater reservoir: State and variability from observations. J Geophys Res. doi:10.1029/2008JC005104

Rabe B, Schauer U, Mackensen A, Karcher M, Beszczynska-Möller A (2009) Freshwater components and transports in Fram Strait–recent observations and changes since the late 1990s. Ocean Sci 5:219–233

Rabe B, Dodd P, Falck E, Schauer U, Mackensen A, Beszczynska-Möller A, Kattner G, Rohling E, Cox K (2013) Liquid export of Arctic freshwater components through Fram Strait 1998–2011. Ocean Sci. doi:10.5194/os-9-91-2013

Rawlins MA, Steele M, Holland MM, Adam JC, Cherry JE, Francis JA, Groisman PA, Hinzman LD, Huntington TG, Kane DL, Kimball JS, Kwok R, Lammers RB, Lee CM, Lettenmaier DP, McDonald KC, Podest E, Pundsack JW, Rudels B, Serreze MC, Shiklomanov A, Skagseth O, Troy TJ, Vörösmarty CJ, Wensnahan M, Wood EF, Woodgate R, Yang D, Zhang K, Zhang T (2010) Analysis of the Arctic System for Freshwater Cycle Intensification: Observations and Expectations. J Clim. doi:10.1175/2010JCLI3421.1

Rigor I, Wallace J, Colony R (2002) Response of Sea Ice to the Arctic Oscillation. J Clim 15:2648–2663

Sein DV, Koldunov NV, Pinto JG, Cabos W (2014) Sensitivity of simulated regional Arctic climate to the choice of coupled model domain. Tellus A. doi:10.3402/tellusa.v66.23966

Sein DV, Mikolajewicz U, Gröger M, Fast I, Cabos W, Pinto JG, Hagemann S, Semmler T, Izqierdo A, Jacob D (2015) Regionally coupled atmosphere-ocean-sea ice-marine biogeochemistry model ROM: 1. JAMES J Adv Model Earth Syst, Description and validation. doi:10.1002/2014MS000357

Serreze MC, Barrett AP, Slater AG, Woodgate RA, Aagaard K, Lammers RB, Steele M, Moritz R, Meredith M, Lee CM (2006) The large-scale freshwater cycle of the Arctic. J Geophys Res. doi:10.1029/2005JC003424

Shiklomanov IA, Lammers R, Peterson B, Vorosmarty C (2000) The Freshwater Budget of the Arctic Ocean. Kluwer Academic Publishers, Netherlands chap The Dynamics of River Water Inflow to the Arctic Ocean

Spreen G, Kern S, Stammer D, Hansen E (2009) Fram Strait sea ice volume export estimated between 2003 and 2008 from satellite data. Geophys Res Lett. doi:10.1029/2009GL039591

Steele M, Morley R, Ermold W (2001) PHC: A Global Ocean Hydrography with a High-Quality Arctic Ocean. J Clim 14:2079–2087

Stroeve JC, Kattsov V, Barrett A, Serreze M, Pavlova T, Holland M, Meier WN (2012) Trends in Arctic sea ice extent from CMIP5, CMIP3 and observations. Geophys Res Lett. doi:10.1029/2012GL052676

Thompson DW, Wallace JM (1998) The Arctic Oscillation signature in the wintertime geopotential height and temperature fields. Geophys Res Lett 25:1297–1300

Tsukernik M, Deser C, Alexander M, Tomas R (2009) Atmospheric forcing of Fram Strait sea ice export: a closer look. Clim Dyn. doi:10.1007/s00382-009-0647-z

Vinje T (2001) Fram Strait Ice Fluxes and Atmospheric Circulation: 1950–2000. J Clim 14:3508–3517

Wadley MR, Bigg GR (2002) Impact of flow through the Canadian Archipelago and Bering Strait on the North Atlantic and Arctic circulation: An ocean modelling study. Q J R Meteorol Soc. doi:10.1256/qj.00.35

Wang J, Zhang J, Watanabe E, Ikeda M, Mizobata K, Walsh JE, Bai X, Wu B (2009) Is the Dipole Anomaly a major driver to record lows in Arctic summer sea ice extent? Geophys Res Lett. doi:10.1029/2008GL036706

Woodgate RA, Aagard K, Weingartner TJ (2006) Interannual changes in the Bering Strait fluxes of volume, heat and freshwater between 1991 and 2004. Geophys Res Lett. doi:10.1029/2006GL026931

Woodgate RA, Lindsay R, Weingartner T, Whitledge T (2009) Bering Strait oceanic fluxes–the Pacific Gateway to the Arctic; part of the NOAA RUSALCA program. FY2009 annual report

Wu B, Wankg J, Walsh J (2005) Dipole Anomaly in the Winter Arctic and Its Association with Sea Ice Motion. J Clim 19:210–225. doi:10.1175/JCLI3619.1

Wu BY, Su J, Zhang R (2011) Effects of autumn-winter Arctic sea ice on winter Siberian High. Chin Sci Bull 56:3220–3228. doi:10.1007/s11434-011-4696-4

Zhang X, Ikeda M, Walsh JE (2003) Arctic Sea Ice and Freshwater Changes Driven by the Atmospheric Leading Mode in a Coupled Sea Ice-Ocean Model. J Clim. doi:10.1175/2758.1